

## Article

# Effect of Hot Filament Chemical Vapor Deposition Filament Distribution on Coated Tools Performance in Milling of Zirconia Ceramics

Louis Luo Fan <sup>1</sup>, Wai Sze Yip <sup>1,2</sup>, Zhanwan Sun <sup>1,3</sup>, Baolong Zhang <sup>1</sup> and Suet To <sup>1,2,\*</sup> 

<sup>1</sup> State Key Laboratory of Ultra-Precision Machining Technology, Department of Industrial and Systems Engineering, The Hong Kong Polytechnic University, Hung Hom, Kowloon, Hong Kong SAR, China; louisluo.fan@connect.polyu.hk (L.L.F.); lenny.ws.yip@polyu.edu.hk (W.S.Y.); zw.sun@gdut.edu.cn (Z.S.); baolong-edison.zhang@connect.polyu.hk (B.Z.)

<sup>2</sup> The Hong Kong Polytechnic University Shenzhen Research Institute, Shenzhen 518063, China

<sup>3</sup> State Key Laboratory of Precision Electronic Manufacturing Technology and Equipment, Guangdong University of Technology, Guangzhou 510006, China

\* Correspondence: sandy.to@polyu.edu.hk

**Abstract:** Zirconia ceramics ( $ZrO_2$ ) have been used for a variety of applications due to their superior physical properties, including in machining tools and dentures. Nonetheless, due to its extreme hardness and brittleness in both sintered and half-sintered forms, zirconia is difficult to machine. In this study, half-sintered zirconia blocks are milled with tungsten carbide milling tools which are coated with diamond film using hot filament chemical vapor deposition (HFCVD) at various substrate-to-filament distances. The objective was to determine the effect of substrate-to-filament distances on the coating thickness, diamond purity, coating grain size, and  $ZrO_2$  machining performance during HFCVD. The experimental results show that, in HFCVD, the grain size and coating thickness of the diamond film on milling tools tend to decrease when the substrate-to-filament distances decrease. Tool failure happened at a cutting time of 200 min for all coated tools. However, the machining quality in terms of surface topology, surface roughness, and tool condition is superior for diamond-coated milling tools with smaller grain sizes and thinner thicknesses. It can be concluded that diamond milling tools with a smaller grain size and lesser thickness produced under shorter substrate-to-filament distances have a superior machining performance and a longer tool life. This study could potentially be used for parameter optimization in the production of coated tools.

**Keywords:** hot filament chemical vapor deposition; diamond-coated tools; micro-milling; zirconia; surface integrity



**Citation:** Fan, L.L.; Yip, W.S.; Sun, Z.; Zhang, B.; To, S. Effect of Hot Filament Chemical Vapor Deposition Filament Distribution on Coated Tools Performance in Milling of Zirconia Ceramics. *Processes* **2023**, *11*, 2773. <https://doi.org/10.3390/pr11092773>

Academic Editor: Hideki KITA

Received: 31 May 2023

Revised: 24 July 2023

Accepted: 31 July 2023

Published: 16 September 2023



**Copyright:** © 2023 by the authors. Licensee MDPI, Basel, Switzerland. This article is an open access article distributed under the terms and conditions of the Creative Commons Attribution (CC BY) license (<https://creativecommons.org/licenses/by/4.0/>).

## 1. Introduction

Zirconia ( $ZrO_2$ ) is an inorganic, non-metallic material with a low thermal conductivity and high chemical inertness; it is mechanical-wear resistant and electrically conductive [1]. Since the mid-1970s, a growing number of nations have increased their efforts and resource allocations into the development of zirconia series products, thereby expanding the functional materials application field of zirconia. As a result of this continuous investment and innovation into zirconia ceramics, it has become one of the highest-performance new materials favored by industrial policies in a number of countries and is widely used in our daily tasks and lives. Zirconia ceramics can be used to manufacture a variety of products for industrial applications, such as machining tools [2], dentures [3], and surface coatings [4], as well as the raw material for telecommunication components, etc.

Numerous technologies exist for machining zirconia ceramics, including laser-assisted machining [5] and abrasive machining [6], but the processing cost is relatively high, the processing efficiency is relatively low, and the precision level of the machined surface is remarkably low. Industrial zirconia ceramics are extremely hard and brittle [7], which

makes large-scale machining challenging. Due to their typical physical and mechanical properties, zirconia ceramic materials can only be initially processed by grinding them under typical conditions.  $ZrO_2$  is a typical zirconia ceramic material that is brittle, posing the greatest challenge to machining. Principally, there are three distinct types of  $ZrO_2$ : pre-sintered, half-sintered, and fully sintered. Due to its extreme hardness and brittleness, it is nearly impossible to machine fully sintered  $ZrO_2$  using conventional methods [8]. Typically, grinding or additional sintering of pre-sintered or partially sintered  $ZrO_2$  is required. Pre-sintered  $ZrO_2$  is significantly softer than other forms of  $ZrO_2$ . In order to obtain observable and quantifiable results, lengthy experiments involving cutting tests are required [9]. This study selected half-sintered  $ZrO_2$  as the cutting material used for the experiments. It is softer than fully sintered  $ZrO_2$  and can still be machined using conventional methods such as milling, but its hardness level is significantly higher than pre-sintered materials. Diamond-coated cutting tools made by h filament chemical vapor deposition (HFCVD) have many excellent properties, including high hardness [9], exceptional thermal conductivity [10], and low friction [11], as well as a low expansion coefficient [12], and this coating technology is considerably less expensive and allows for greater flexibility in tool geometry. The diamond-coated tools for zirconia ceramic workpiece machining are anticipated to have a significantly longer tool life and produce a superior machining quality than that of non-coated tools.

Numerous studies have investigated the connection between various parameters and coating performance. Numerous experiments were conducted to determine the effects of the influential factors of HFCVD, such as pretreatment strategies, methane concentration, chamber pressure, and reaction temperature. Due to the vast difference between the filament temperature and the background temperature of the furnace, there is a sharp temperature gradient between the hot filament and the substrate during HFCVD. In addition, because the temperature range for the synthesis of  $sp^3$  carbon bonding is very narrow, a slight change in the substrate-to-filament distance has a significant impact on the purity and surface morphology of the diamond coating. Nevertheless, a clear illustration of the effect of the substrate-to-filament distance on the milling performance of diamond-coated tools on semi-sintered zirconia ceramics is still lacking. Therefore, the purpose of this paper is to determine the relationship between the milling performance of zirconia with HFCVD-coated tools and the substrate-to-filament distance in the HFCVD process. The coating parameters, particularly the substrate-to-filament distance, of an HFCVD-coated tool for milling zirconia are chosen as the main variables within a series of experiments conducted with different cutting parameters. This helps in determining the optimal cutting parameter for various tolerance and application requirements in order to maximize tool life while maintaining the required energy efficiencies and surface finishes.

In this paper, the structure is organized as follows: Section 2 introduces the procedures and mechanisms of HFCVD diamond coating and  $ZrO_2$ . Section 3 illustrates the experimental setup of the HFCVD process and  $ZrO_2$  cutting test. Section 4, explains the results and discussion including the effect that the distance between the substrate and filament had on the grain size, the coating thickness of HFCVD-coated milling tools, the purity of  $sp^3$  carbon within diamond coated milling tools, tool wear, and surface quality. Lastly, Section 5 summarizes and concludes this study.

## 2. Theory

### 2.1. Decarburization and Cobalt Etching in HFCVD Diamond Coating

Cobalt granules are typically added to the powder metallurgy process in order to bind tungsten carbide rods and tools. This is due to the high solubility of carbon with transition elements such as cobalt during the HFCVD diamond synthesis process; cobalt induces graphitization during the formation of the diamond deposit, reducing the purity of the diamond coating and the adhesion strength between the diamond coating and the tungsten carbide substrate surface [13]. Gaseous cobalt diffuses into the diamond coating during the diamond deposition process in HFCVD, increasing the yield of  $sp^2$

bonding (graphite phase) and decreasing the yield of  $sp^3$  bonding. In contrast to deposition on the substrate surface, carbon would diffuse into the cobalt granules in the carbide substrate [14]. To prevent or reduce the negative effects of cobalt and carbon diffusion, a series of pretreatments involving Murakami etching and nitric acid etching must be performed prior to the HFCVD process to remove surface and subsurface cobalt.

### 2.2. The Effect of Substrate to Filament Distance in HFCVD Coating Process

HFCVD is widely utilized in industries for diamond synthesis applications. However, there are a number of deposition parameters in HFCVD that have a significant effect on the surface morphology and growth rate of the diamond film. In the HFCVD process, when the concentration of  $CH_4$  near the filament rises due to the flow of methane, the concentration of the methyl radical ( $CH_3$ ) rises, which diffuses onto the surface of the substrate. The  $CH_3$  further reacts with hydrogen ions to produce methanide radicals ( $CH_2$ ) and methylidyne radicals ( $CH$ ), which ultimately reduce to carbon atoms and are deposited on the substrate to facilitate diamond nucleation and growth. In addition, the increase in  $CH_4$  concentration encourages secondary nucleation, which decreases grain size [15]. On the surface of the crystals formed by the initial nucleation, a second nucleus forms, inhibiting their growth. Furthermore, the second nuclei smoothen the surface by filling any surface irregularities [16]. This indicates that as methane flow increases, growth rate will increase while grain size will decrease [15,16].

As for the effect of  $H_2$  concentration in the HFCVD process, it is closely related to the concentration of hydrogen ions, which is necessary for receiving the hydrogen ions released during the previously mentioned methane fragmentation. In addition, it eliminates  $sp^2$  carbon, which reduces the yield of graphite and other carbon forms that are not diamonds. When the concentration of  $H_2$  reaches a critical level, the  $sp^3$  carbon will also be etched away at a rate faster than the diamond nucleation and deposition rates, thereby inhibiting the nucleation and growth of diamond crystals [17].

The concentration gradient of  $CH_3$ ,  $CH_2$ , and  $CH$  decreases with an increasing distance between the substrate and the filament. Therefore, as the substrate approaches the filament, it is exposed to a greater concentration of  $CH_3$ ,  $CH_2$ , and  $CH$  radicals and a shorter diffusion distance, which increases surface diffusion on the substrate's surface. This improves the growth rate of the diamond film. However, the substrate's temperature increases when it is close to the filament. Since  $sp^3$  carbon can only form within a relatively narrow temperature range, placing the substrate too close to the filament may impede diamond growth.

### 2.3. $ZrO_2$ Cutting Mechanism

Due to the high hardness of  $ZrO_2$ , the main material removal mechanism of sintered  $ZrO_2$  is focused on its brittle or semi-brittle nature. In addition to removal via brittle fracture mode,  $ZrO_2$  can be removed via plastic deformation under the cutting conditions of a low feed rate and a high spindle speed [18–20].

Under the case of micro milling with a ball end mill, the cutting speed,  $v_c$ , can be calculated using Equation (1) when the value of the inclination angle of the tool axis  $\beta$  is zero (vertical milling), as shown below,

$$v_c = 2\pi n \sqrt{a_p(D - a_p)}, \quad \text{where } \beta = 0 \quad (1)$$

where  $n$  is the spindle speed,  $D$  is the tool diameter and  $a_p$  is the axial the depth of cut [21] (Figure 1).

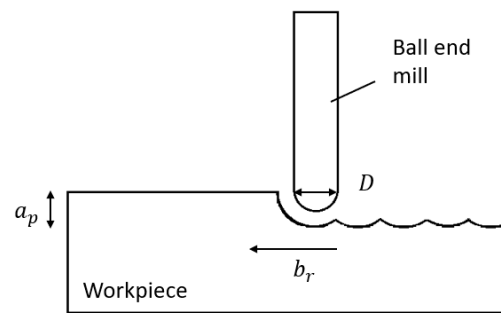


**Figure 1.** Kinematics of vertical micro-ball end milling.

The chip formation and tool wear during the zirconium micro-milling process are simplified and summarized for clarity in Figure 2. Due to the brittleness of zirconium, the cutting chips of it in micro-milling are discontinuous [22]. The tool wear that develops during a process can be divided into three stages, the first stage consists of abrasive and adhesive wear, in which coating dents caused by abrasive wear allow residue materials from the workpiece to adhere to the coating surface [23]. The second stage of tool wear is characterized by attrition wear and apparent delamination of coating [24]. The indentations formed during the first stage enhance the formation of cracks caused by debonding, resulting in coating delamination. In the third and final stage of tool wear, the coating has completely delaminated, exposing the substrate material and resulting in abrasive wear on the substrate [25] which causes tool failure [26].

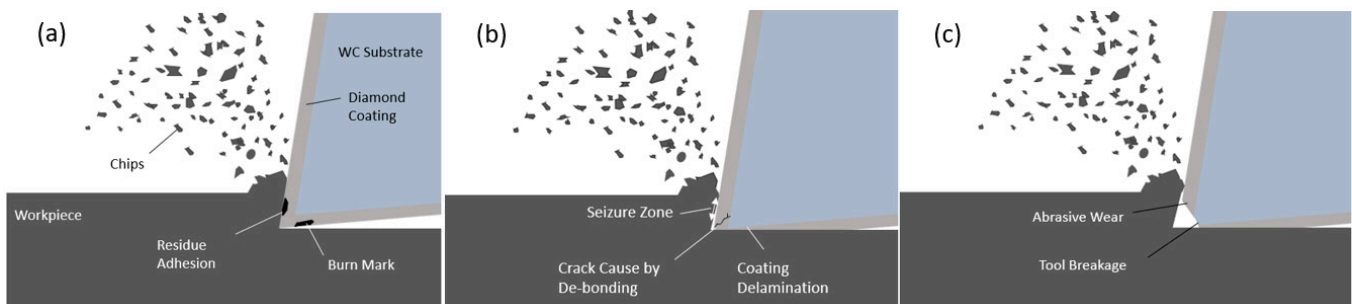


**Figure 2.** Three main stages of tool wear (a) stage 1: adhesive and abrasive wear, (b) attrition wear and delamination, (c) substrate material breakage.

### 3. Experimental Setup

Uncoated tungsten carbide ball end mills (diameter: 2 mm, flute length: 12 mm, overall length: 50 mm, outer diameter: 4 mm) were chemically pretreated before HFCVD diamond deposition. The tools were first treated with Murakami solution (85% KOH: 99.5%  $K_3[Fe(CN)_6]$ :  $H_2O$ , 1:1:10) to increase surface roughness and improve mechanical interlocking between the substrate and HFCVD-deposited diamond layer. Before the second pretreatment, the instruments were cleaned and dried. The instruments were ultrasonically etched in a 98%  $HNO_3$ : $H_2O$ , 1:10 solution for cobalt removal.

Following the cobalt etching of the ball end mills, a seeding procedure was carried out to facilitate the nucleation of diamond during the initial phase of the diamond deposition. The instruments were treated in an ultrasonic bath for 30 min with a 3–6 micron diamond powder ethanol solution, followed by a 30 second treatment with 99 percent ethanol to remove excess diamond powder. The tools were then placed within the HFCVD furnace. The tools were divided into two sets, A and B, with substrate-to-filament distances 10 and 30, respectively. The parameter for HFCVD coating is shown in Table 1. After the HFCVD diamond deposition on the milling tools, the tools performed scanning electron microscopy (SEM) imaging and Raman analysis to determine their various coating properties, such as coating grain size, coating thickness, and the percentage of  $sp^3$  bonds present in the

coatings produced. Figure 3 shows the HFCVD machine and related facilities used in this study for the diamond coating of drilling tools.

**Table 1.** HFCVD Deposition Parameters.

Deposition Set	Cobalt Etching Time (min)	Seeding (min)	CH <sub>4</sub> Flow (sccm)	H <sub>2</sub> Flow (sccm)	Substrate Distance from Filament (mm)	Chamber Pressure (mbar)	Power (kW)
A	6	20	2000	30	10	10	4
B	6	20	2000	30	30	10	4

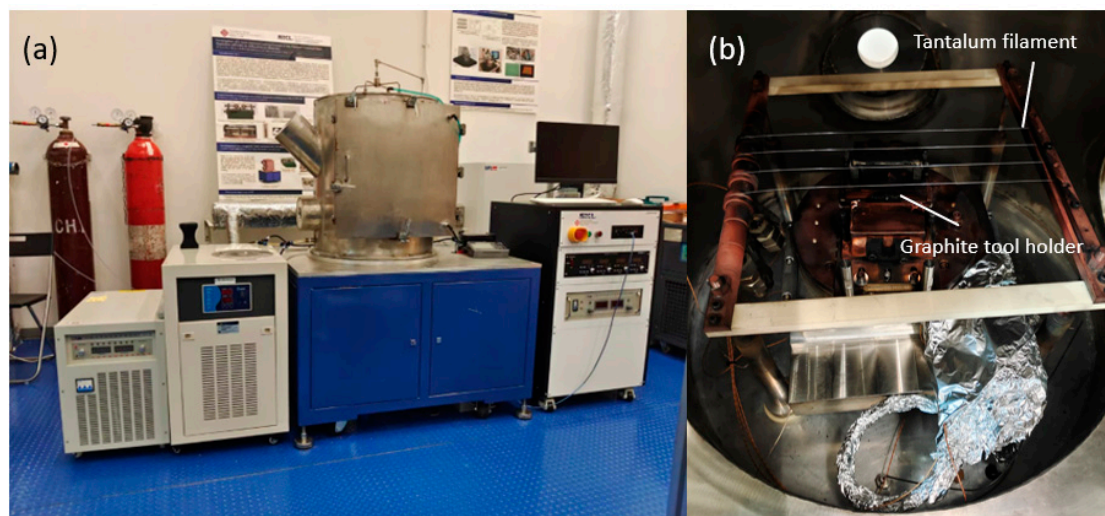


**Figure 3.** The HFCVD and the related facilities for diamond coating of drilling tools, (a) overall installation of HFCVD facilities, (b) inner view of HFCVD reaction chamber.

Twelve diamond-coated milling tools (six milling tools from set A and six milling tools from set B) were then used to conduct a series of ZrO<sub>2</sub> cutting tests with the following parameters: spindle speed of 22 krpm, feed rates of 100 mm/min and 200 mm/min, cutting times of 200 min, 400 min, and 800 min, and a depth of cut of 0.6 mm. The sample size was 30 mm × 20 mm. Table 2 includes the cutting parameters. After the cutting tests, the ZrO<sub>2</sub> workpiece surface was analyzed by an optical profiling system to determine surface roughness and surface profile in order to deduce the cutting quality of coated end mills manufactured under two different substrate-to-filament distances in relation to the different cutting parameters.

**Table 2.** ZrO<sub>2</sub> Milling Parameters.

Sample	Spindle Speed (krpm)	Feed Rate (mm/min)	Cutting Time (min)	Depth of Cut (mm)
1	22	100	200	0.6
2	22	100	400	0.6
3	22	100	800	0.6
4	22	200	200	0.6
5	22	200	400	0.6
6	22	200	800	0.6

## 4. Result and Discussion

### 4.1. The Effects of Distance between Substrate and Filament on Grain Size and Coating Thickness of HFCVD Coated Milling Tools

Figure 1a–d are SEM images of the coating produced using deposition on set A and set B tools, respectively. According to Figure 4, the average grain size of the coating produced

using deposition for set B is  $9.37\ \mu\text{m}$ , which is considerably larger than the grains produced using deposition for set A, which are only  $3.19\ \mu\text{m}$ . In terms of coating thickness, the coating produced using deposition for set B has an average grain size of  $43.56\ \mu\text{m}$ , which is approximately  $5.77\ \mu\text{m}$  thicker than the coating produced using deposition for set A. The SEM results indicate that the coating thickness increases as grain size increases. As a result of the growth rate during diamond deposition, the growth rate obtained using deposition for set B is considerably higher than for set A. When coated tools are produced under the coating parameters for set A at a shorter substrate-to-filament distance, the surface of the substrate is exposed to a higher concentration of  $\text{CH}_3$ ,  $\text{CH}_2$ , and  $\text{CH}$  radicals, the carbon sources for diamond synthesis. This should theoretically increase the growth rate. However, the substrate's temperature increases when it is close to the filament. Due to the fact that  $\text{sp}^3$  carbon can only form within a narrow temperature range [27], when the substrate is too close to the filament the substrate temperature would exceed the optimal temperature for diamond synthesis, reducing the growth rate and the coating purity [28], which causes the thinner coating thickness and smaller grain size for the milling tools in set A. In addition, the increased concentration of  $\text{CH}_3$ ,  $\text{CH}_2$ , and  $\text{CH}$  radicals resulting from the coating parameters of set A promotes secondary nucleation, resulting in a smaller average grain size compared to set B. In conclusion, when the distance between the substrate and the filament decreases in HFCVD processes, the grain size and coating thickness of the diamond film on milling tools become generally smaller and thinner.

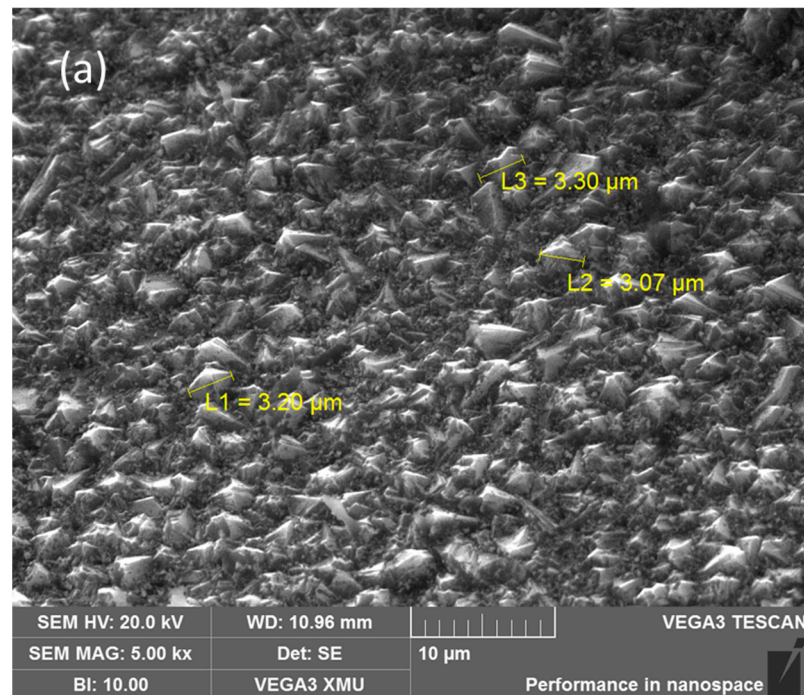


Figure 4. Cont.

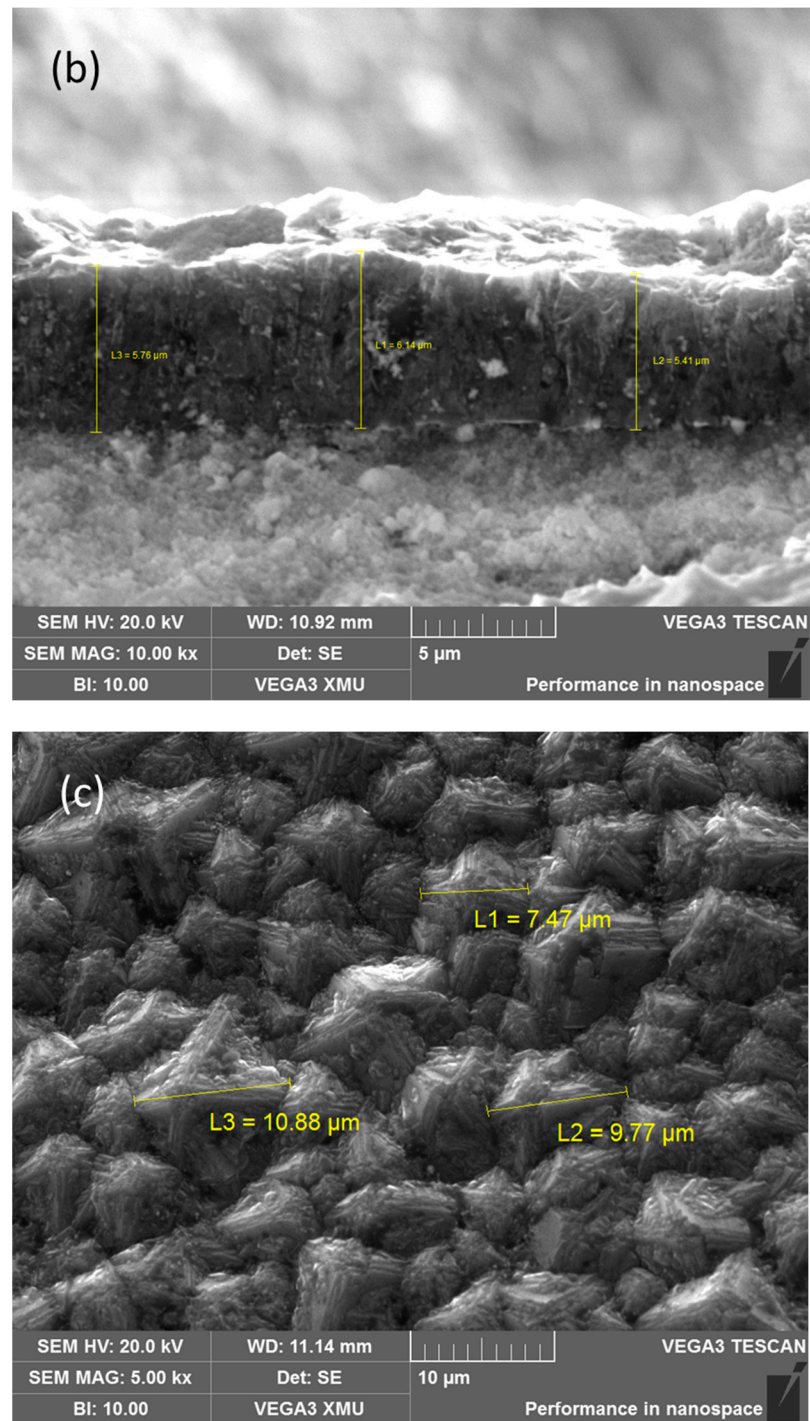
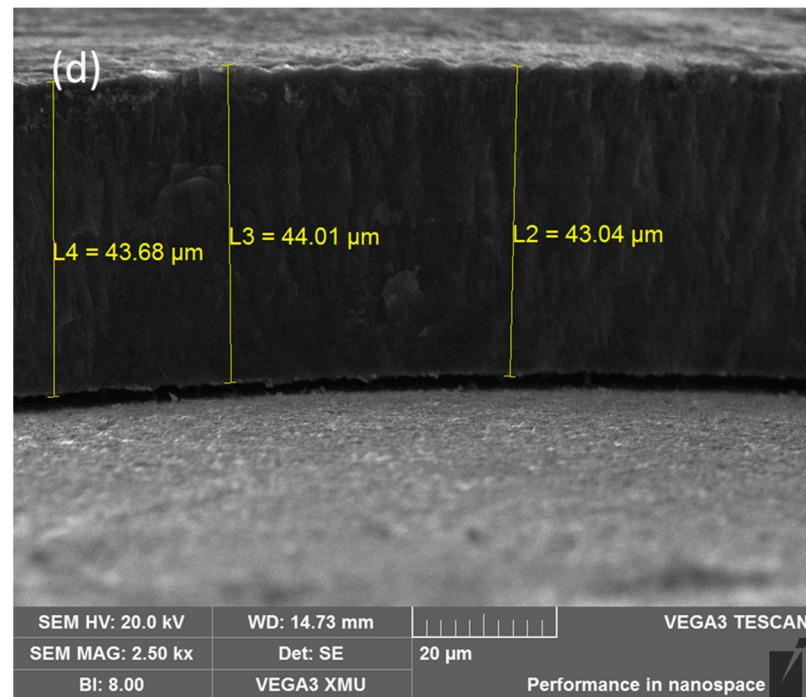


Figure 4. Cont.



**Figure 4.** SEM images of diamond-coated tools produced by HFCVD under set A (a) grain size, (b) coating thickness, and set B (c) grain size, (d) coating thickness.

#### 4.2. The Effects of Distance between Substrate and Filament on the Purity of $sp^3$ Carbon of Diamond-Coated Milling Tools

Raman spectroscopy is a nondestructive technique for analyzing materials based on the interaction between light and the material. Raman spectroscopy can provide detailed information about the chemical structure, phase and morphology, crystallinity, and molecular interactions of the coated milling tools. Typically, a Raman spectrum comprises a certain number of Raman peaks, each of which represents the wavelength position and intensity of the Raman scattered light corresponding to that peak. For each peak, a particular molecular bond vibration can be identified.

With the Renishaw Micro-Raman Spectroscopy System<sup>TM</sup>, it is possible to obtain Raman spectrograms of the diamond coating for tools in sets A and B, displaying the intensity distributions of various characteristic peaks as illustrated in Figures 5 and 6, respectively. Multiple peak fitting based on the Gaussian model clearly demonstrates the composition of the coating, which consists of disordered  $sp^3$  carbon, C-N vibrations, diamond, disordered graphite, distorted  $sp^3$  carbon, graphite, etc. Once all the relevant characteristic peaks have been identified, as shown in Tables 3 and 4 which show the Raman spectra for the peak fitting of diamond-coated milling tools for both sets A and B, the area of integration can be calculated for quantitative analysis. The purity of  $sp^3$  carbon in set A can be calculated to be approximately 98.47 percent when  $sp^2$  and  $sp^3$  carbon are added together. In contrast, the  $sp^3$  purity of set B exceeds 99 percent. Comparing the  $sp^3$  proportion results, one can conclude that for an increase in the distance between the substrate and the filament in a HFCVD process, the purity of the  $sp^3$  carbon in the diamond-coated milling tools is improved.

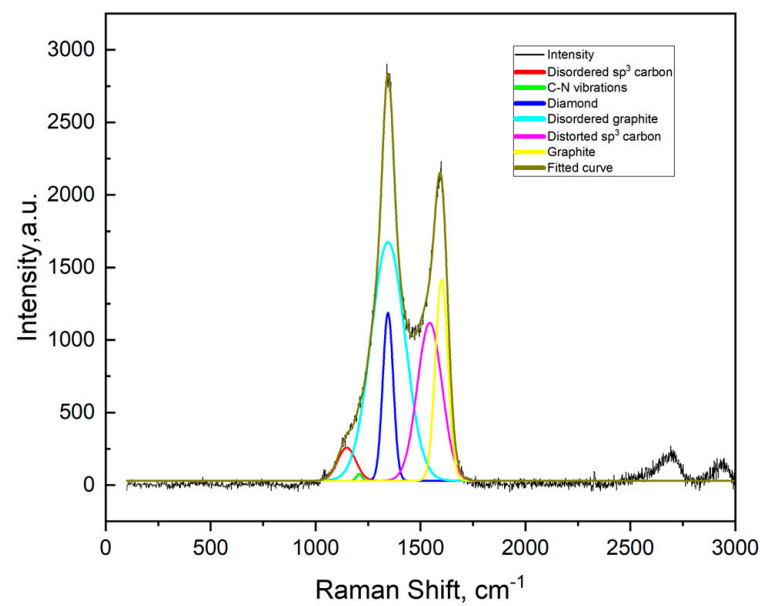


Figure 5. Raman spectrum for peak fitting of diamond-coated milling tools of set A.

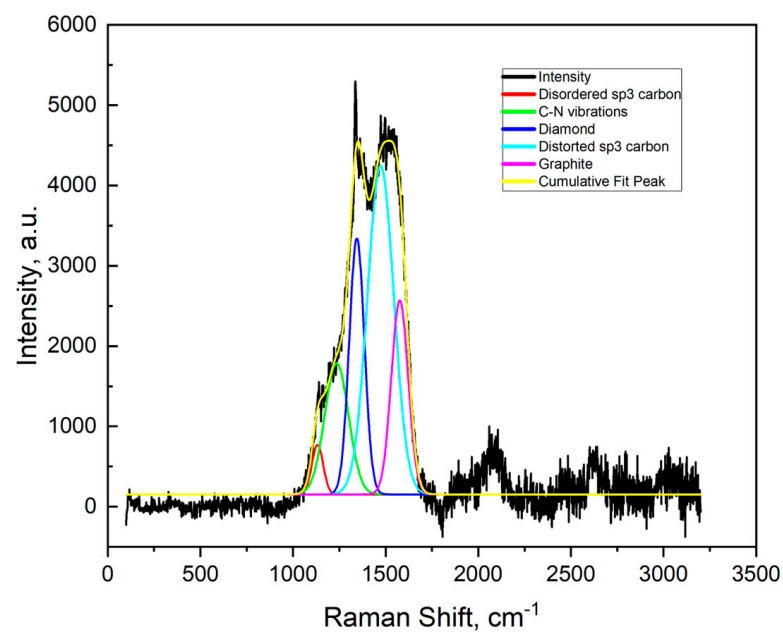


Figure 6. Raman spectrum peak fitting of diamond-coated milling tools of set B.

Table 3. Integration results for peak fitting of diamond-coated milling tools of set A.

Assignment	Area of Integration
Disordered $sp^3$ carbon	117,832
C-N vibrations	94,698
Diamond	164,886
Disordered graphite	427,524
Distorted $sp^3$ carbon	253,574
Graphite	197,225
$Sp^3/sp^2$	64.3809
$Sp^3$ purity	0.9847

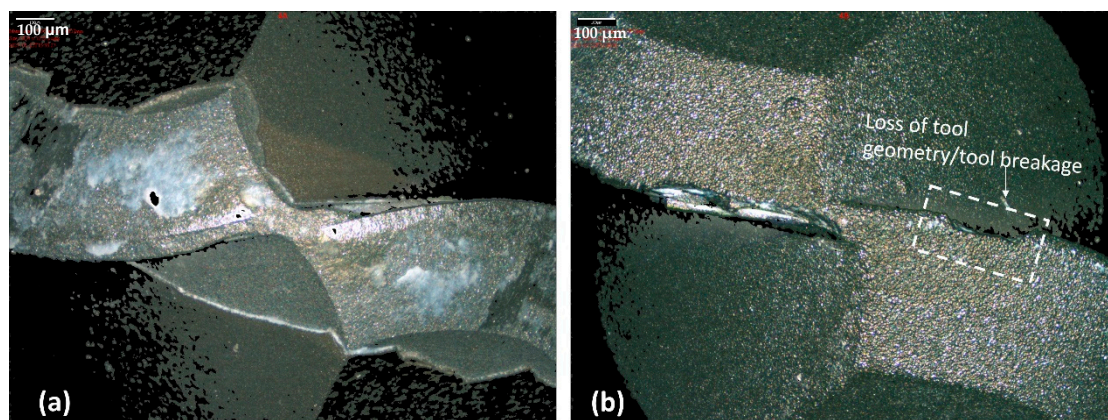
**Table 4.** Integration result for peak fitting of diamond-coated milling tools of set B.

Assignment	Area of Integration
Disordered sp <sup>3</sup> carbon	523,629
C-N vibrations	738,764
Diamond	801,438
Distorted sp <sup>3</sup> carbon	1,203,299
Graphite	750,086
Sp <sup>3</sup> /sp <sup>2</sup>	252.8075
Sp <sup>3</sup> purity	0.9961

#### 4.3. The Effects of Distance between Substrate and Filament on Tool Wear

The progression of tool wear for a diamond-coated tool during milling includes the adhesive wear, delamination of coated materials, tool breakage/loss of tools, and the geometry of the coated and substrate materials, according to the cutting mechanism of a diamond-coated tool [29]. High cutting temperature causes a continuous adhesion of workpiece materials, to the rake and flank faces of the cutting tool at first. As a result, the relief angle of the cutting edge decreases, and the cutting motion changes to plowing and rubbing. Abrasive wear increases as a result of the constant compression stress, friction heat, and high cutting temperature. During continuous cutting, delamination occurs along the cutting edge of a coated tool, exposing the sharp edge of the tool substrate. The wear process may include graphitization in the diamond at high cutting temperatures, as well as attrition in columnar diamond grains. As a result of the constant cutting, the exposed tungsten carbide edge quickly wore away. This results in a variation in the tool geometry, rounding of the cutting edge, and tool breakage.

A similar logic is applied to the ball end mill conditions in this study. Figure 7 illustrates SEM images of ball end mills from sets A and B, which the cutting time is 200 min. According to Figure 7, an end mill tool edge from set A shows a shiny surface on the drilling edges, indicating that the tungsten carbide substrate has already been exposed; however, it is not yet to the stage of tool breakage. For the end mill tool edge of set B, however, the tool breakage has already occurred at the same cutting time as the drilling tool of set A. As shown in Figure 7b, a variation in the tool geometry has been observed on the drilling edge. As a result, under the same cutting conditions, the drilling tool of set B has tool breakage, whereas the end mill tool of set A is still in the delamination stage, demonstrating that the tool wear level of set A is lower than that of set B. The aforementioned testing results demonstrated that the milling tools of set B have already failed at 200 min of cutting, but the milling tools of set A are still able to continue cutting.

**Figure 7.** SEM images of drilling tools from (a) set A, and (b) set B, for cutting time 200 min.

#### 4.4. Influence of Distance between Substrate and Filament on Surface Quality

Table 5 summarized the surface roughness of milled surfaces by diamond-coated milling tools for sets A and B. Figure 8 indicates that a higher feed rate (200 mm/min) in milling of zirconia ceramic using diamond-coated milling tools results in a lower average surface roughness value, particularly when the cutting time is at 200 min. This is because larger grain size experiences more severe friction, thus experiences more wear under high spindle speed [30]. Moreover, film cracks tend to propagate through the columnar particles, leading to a decrease in toughness and adhesion. This result is consistent with the tool condition described in Section 4.1, which indicates that set B milling tools failed at 200 min. On the other hand, the reason that set A and set B tools have comparable surface roughness at 800 min is because both sets have experienced significant tool wear as a result of prolonged machining time.

**Table 5.** Surface roughness of milled surfaces by diamond-coated milling tools for sets A and B.

Sample	Surface Roughness (nm)	
	Set A	Set B
1	470.667	620.667
2	405.667	949.333
3	478.333	235.333
4	395.333	618.667
5	159.667	487.666
6	423.667	360

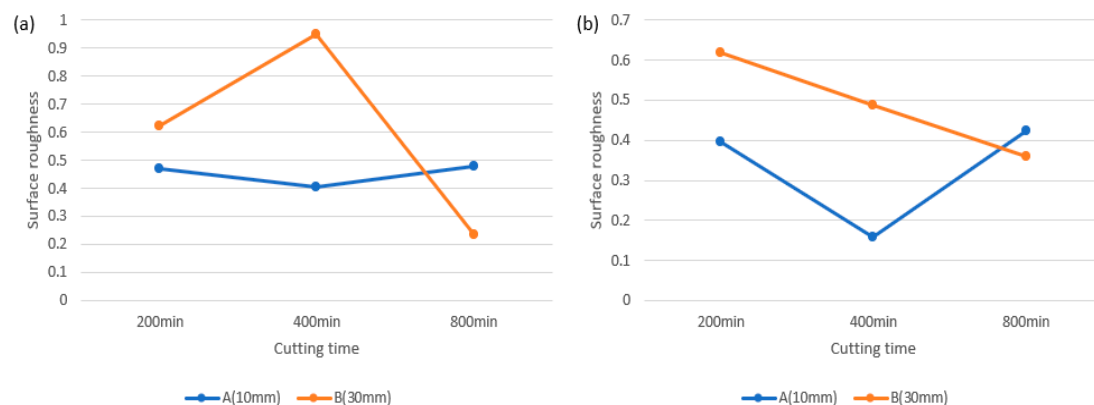


**Figure 8.** Surface roughness vs. cutting time for sets A and B diamond milling tools (a) at feed rate 100 mm/min and, (b) 200 mm/min.

To comprehend the effect of substrate-to-filament distance on the cutting quality of coated end mills under different cutting parameters, it is necessary to examine the average surface roughness. Figure 9 indicates that a higher feed rate (200 mm/min) results in a lower surface roughness value for both set A and B diamond-coated milling tools, particularly when the cutting time is 400 min. Comparing the surface produced by set A and set B, the surface roughness of the machined surface of a diamond-coated milling tool from set B is significantly higher than that of a tool from set A due to the larger grain size, which causes the individual grains and the coating to experience a higher level of stress during the milling process. As mentioned above, under the larger microcrystalline diamond (MCD) structure, film cracks propagate through the columnar particles; a thicker coating has longer columnar particles which further enhance crack propagation, reducing the adhesion and toughness of the coating [31]. However, for a smaller grain size coating such as the diamond coating produced using deposition for set A, the structure is less continuous, thus reducing crack propagation. In addition, tool wear increases with the grain size [29] and the substrate material, tungsten carbide, is brittle, resulting in the accumulation of

internal stress along the coating, interlayer, and substrate subsurface. This causes tool delamination and even abrasive wear, resulting in severe tool wear or even the failure of the diamond-coated milling tools of set B. At 800 min, both set A and set B tools had a similar surface roughness distribution, as both sets had already experienced significant tool wear and failure.

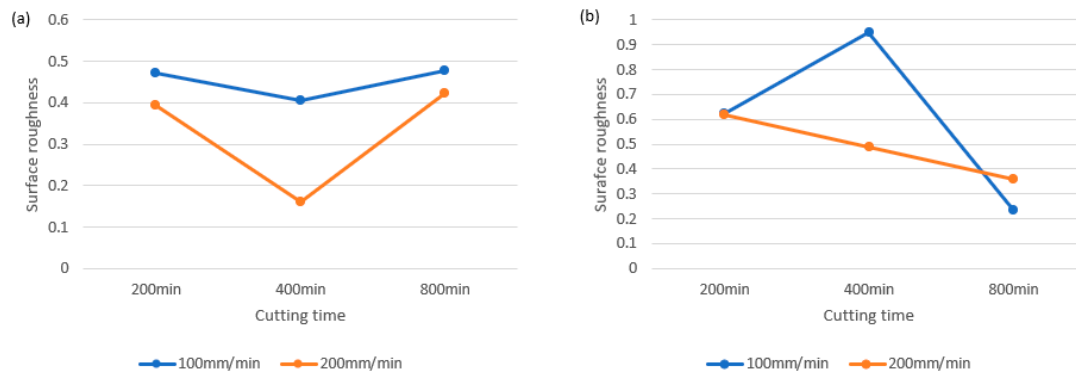


**Figure 9.** Surface roughness against cutting time at 100 mm/min and 200 mm/min feed rates (a) set A diamond milling tools and, (b) set B diamond milling tools.

Figure 10 shows the surface topology of the surface machined with set A and B diamond milling tools at a feed rate of 100 mm/min and 200 mm/min for 200 min, 400 min and 800 min, respectively. Due to peeling of the zirconia ceramic surface in milling, the machined surfaces produced by set B diamond-coated milling tools exhibit numerous micro-voids and cavities, which are evenly distributed on the machined surface. The micro-void on the machined surface is a typical surface defect that appeared during tool milling with a diamond-coated tool. These voids can serve as sites for crack initiation, leading to the collapse of near-surface cavities and the initiation and propagation of cracks along grain boundaries [32]. As a result, a network of various voids is found on the surface which causes stress concentration on the machined surfaces, which in turn affects the mechanical properties of components made with a diamond-coated milling zirconia surface. As mentioned above, the larger grain size and thicker coating of set B diamond-coated tools promote crack propagation and mean that they experience a larger internal stress which leads to tool failure and reduces the cutting quality. In conclusion, the diamond-coated milling tool from set A produces a surface with fewer surface defects. In conjunction with the results and justification of surface roughness in Sections 4.2 and 4.3, it can be concluded that a diamond-coated tool with an appropriately thin coating thickness and finer grain size produces a machined surface with a higher quality, and that a shorter substrate-to-filament distance will produce a surface with higher quality on zirconia ceramics.

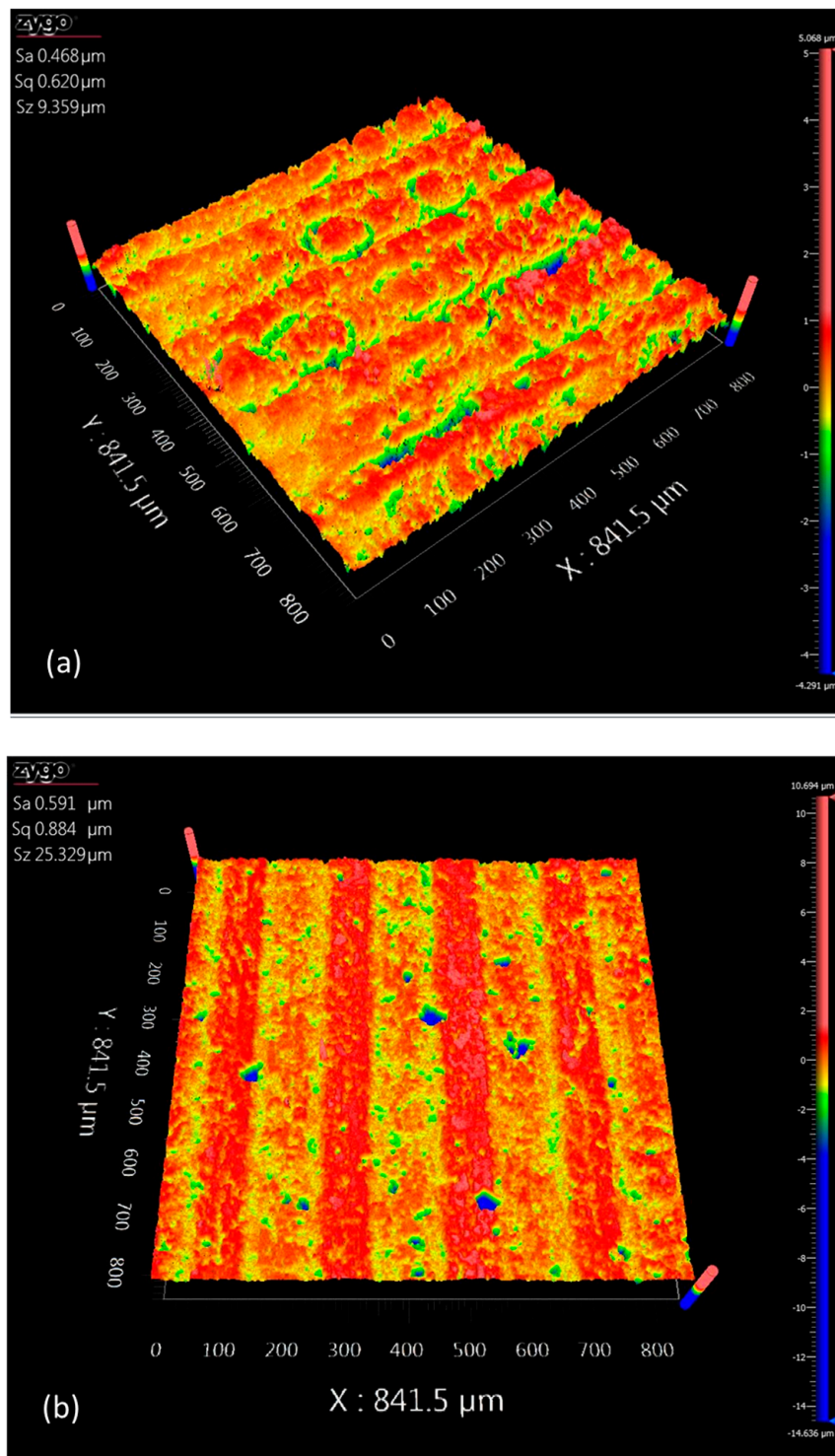


Figure 10. Cont.

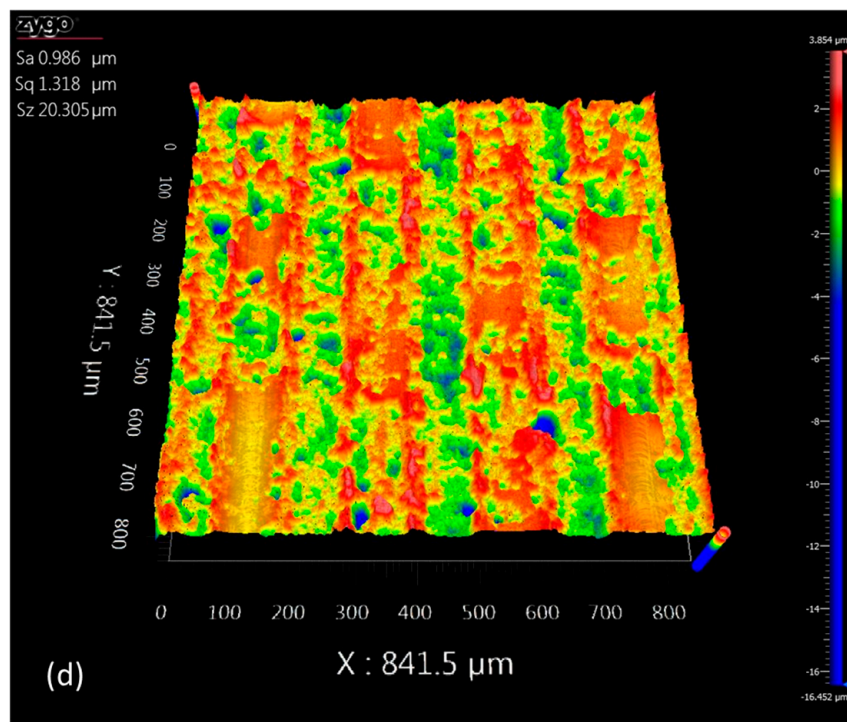
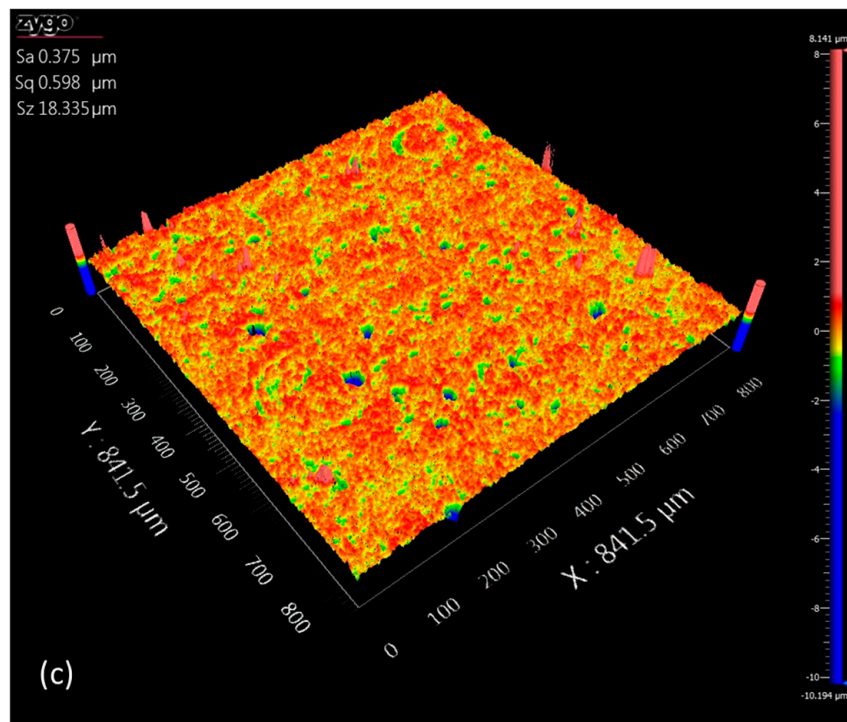


Figure 10. Cont.

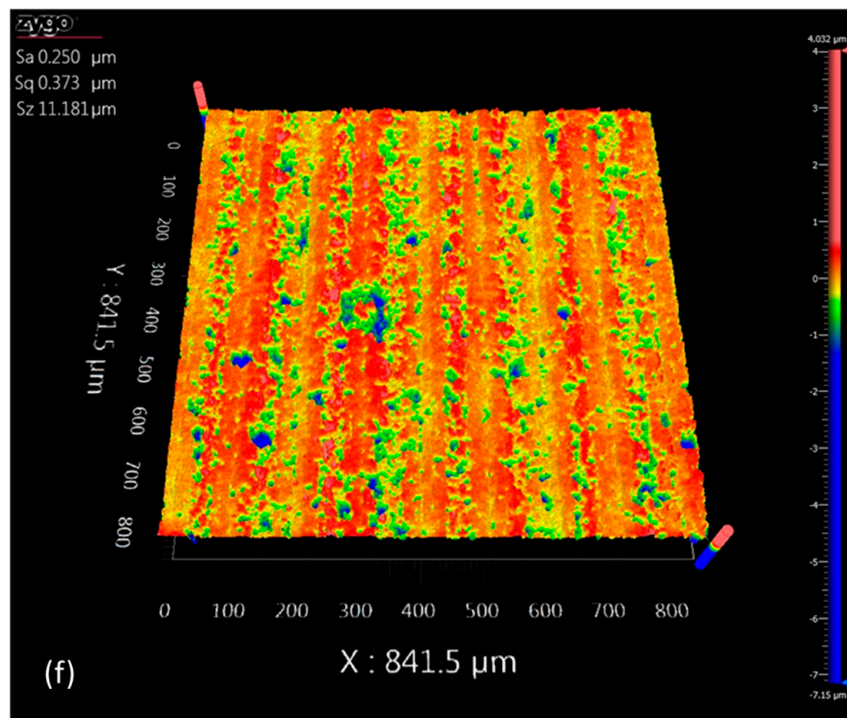
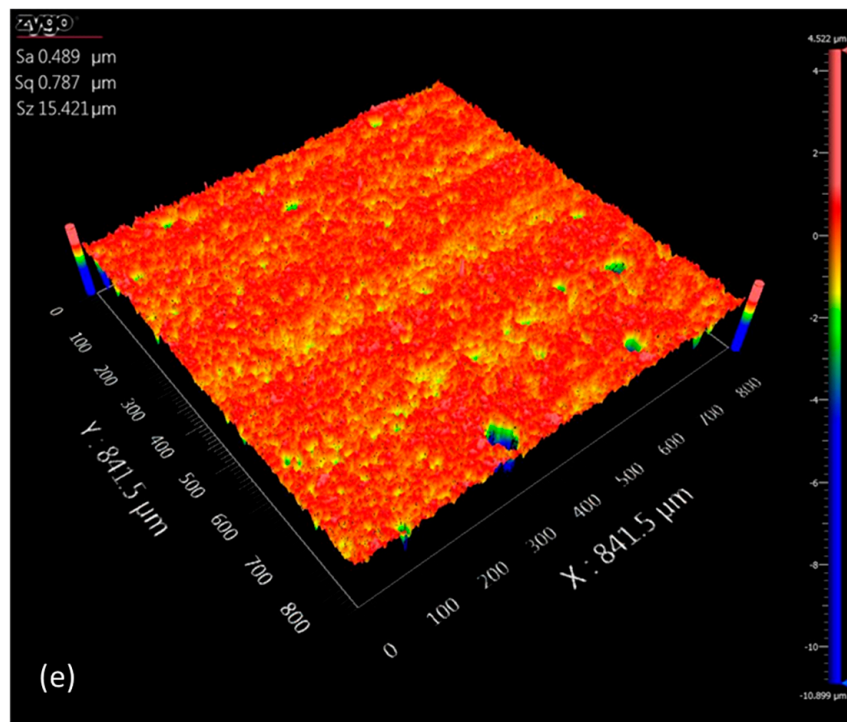


Figure 10. Cont.

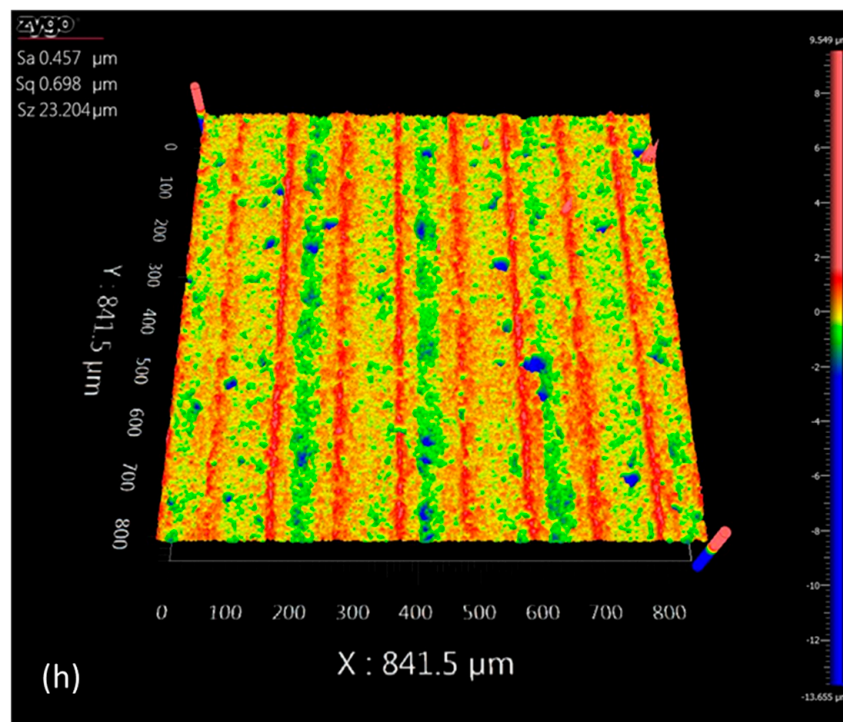
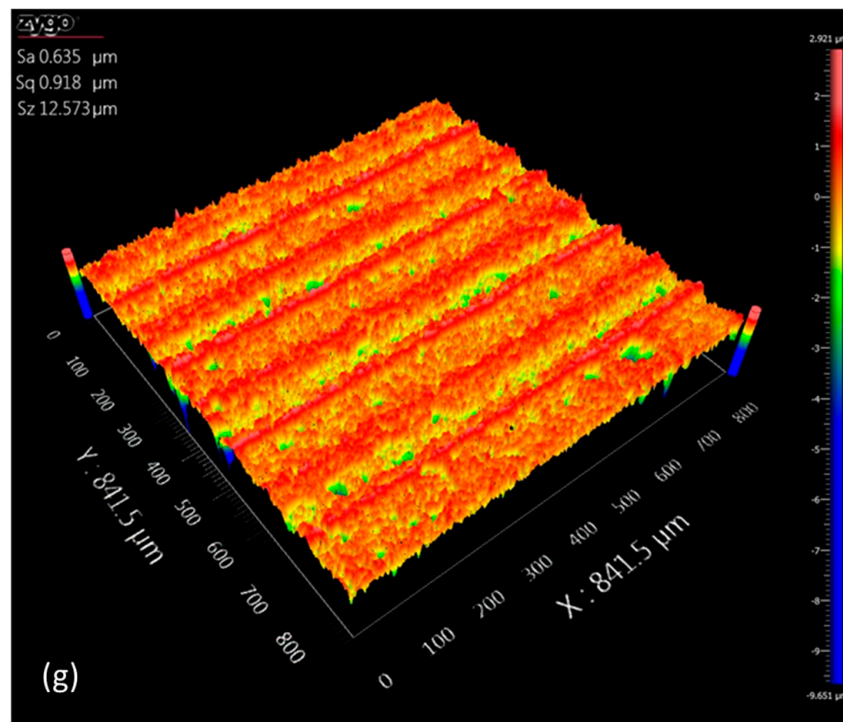


Figure 10. Cont.

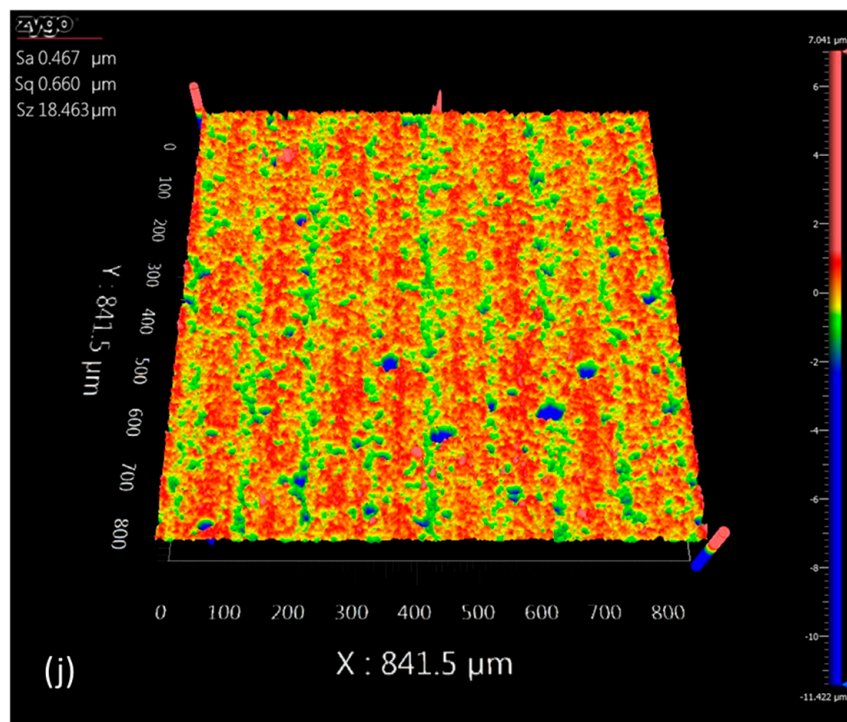
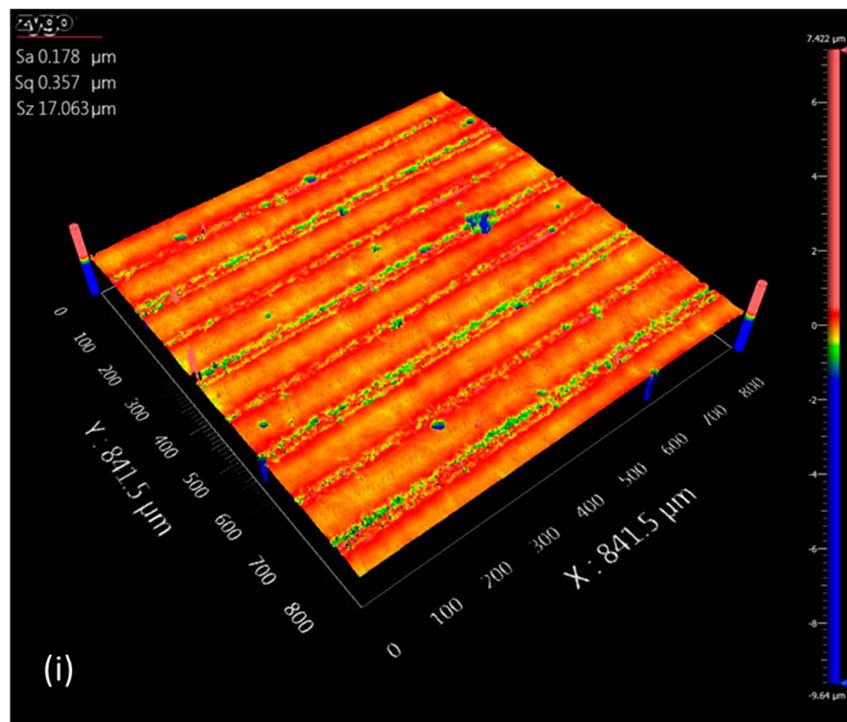
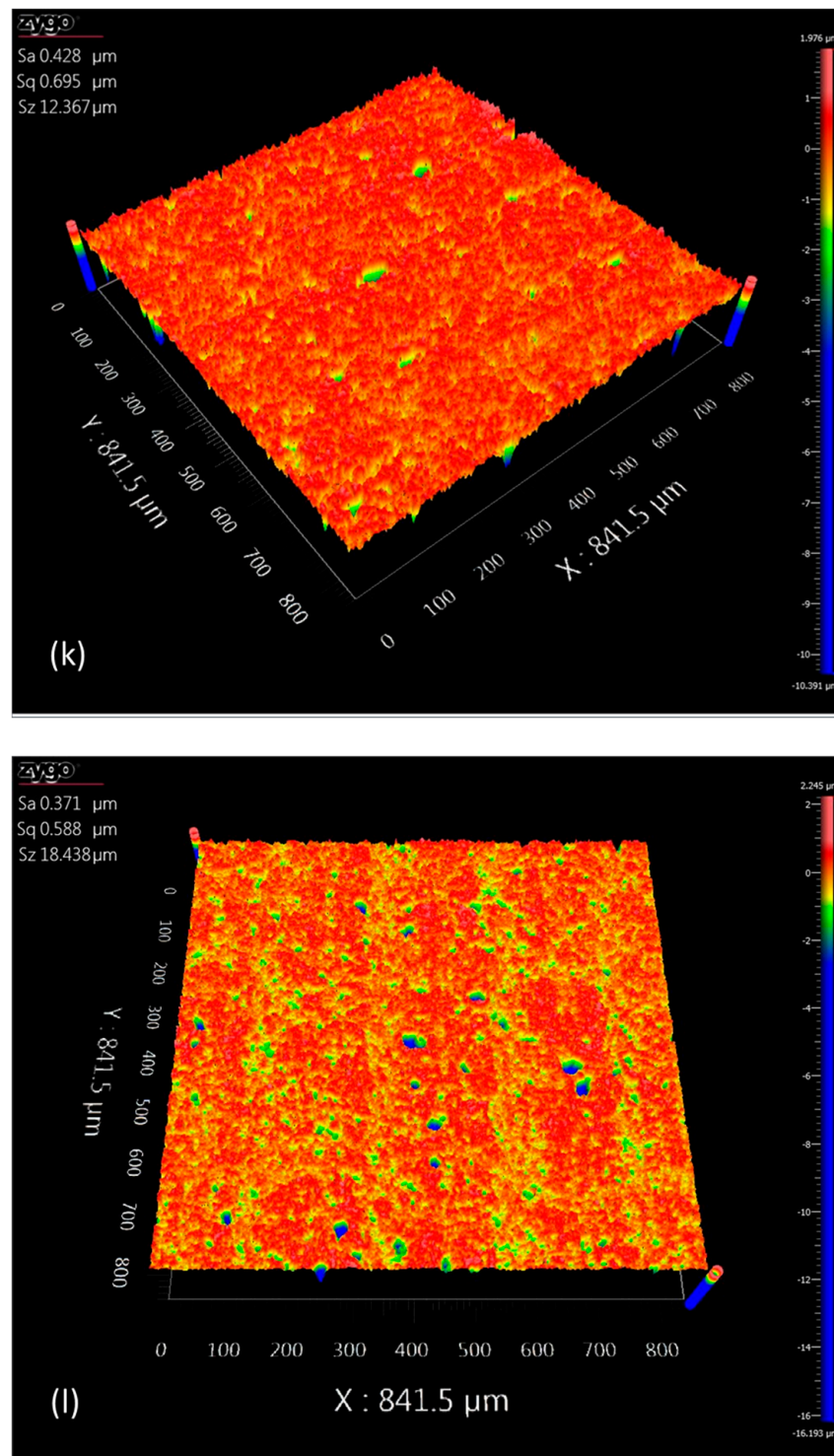


Figure 10. Cont.



**Figure 10.** 3D profile images of zirconia surface machined by diamond-coated milling tools from set A, feed rate: 100 mm/min (a) cutting time: 200 min, (c) cutting time: 400 min, (e) cutting time: 800 min; feed rate: 200 mm/min, (g) cutting time: 200 min, (i) cutting time: 400 min, (k) cutting time: 800 min and set B, feed rate: 100 mm/min, (b) cutting time: 200 min, (d) cutting time: 400 min, (f) cutting time: 800 min; feed rate: 200 mm/min, (h) cutting time: 200 min, (j) cutting time: 400 min, (l) cutting time: 400 min.

## 5. Conclusions

In this work, half-sintered zirconia blocks are milled using tungsten carbide milling tools coated by varied substrate-to-filament distances in HFCVD. The goal is to investigate the influence of substrate-to-filament distance in an HFCVD process on coating grain size, coating thickness, diamond purity, and ZrO<sub>2</sub> machinability. This research implies that milling tools produced with shorter substrate-to-filament distances have a better tool life and milling performance on ZrO<sub>2</sub> ceramics; the findings are summarized below.

- a. Shorter substrate-to-filament distances lead to a smaller grain size and a thinner coating thickness due to excessively high temperatures and secondary nucleation.
- b. Shorter substrate to filament distances lead to a lower diamond purity of the coating.
- c. Tools with coating produced under a shorter substrate-to-filament distance are less prone towards tool breakage.
- d. An appropriately thin coating and fine grain size from a shorter substrate-to-filament distance produces a better machined surface with far less micro-voids and cavities.

**Author Contributions:** Conceptualization, L.L.F.; Methodology, L.L.F.; Software, L.L.F. and B.Z.; Validation, W.S.Y. and S.T.; Formal analysis, L.L.F.; Investigation, L.L.F. and Z.S.; Resources, Z.S. and S.T.; Data curation, L.L.F., Z.S. and B.Z.; Writing—original draft, L.L.F. and B.Z.; Writing—review & editing, W.S.Y.; Visualization, B.Z.; Supervision, W.S.Y. and S.T.; Project administration, S.T.; Funding acquisition, S.T. All authors have read and agreed to the published version of the manuscript.

**Funding:** The work described in this paper was partially supported by a grant from the General Research Fund from the Research Grants Council of the Hong Kong Special Administrative Region (Grant number PolyU15221322); the major project of the National Natural Science Foundation of China (Project No.: U19A20104); Shenzhen Science and Technology Program (Project No.: JCYJ20210324131214039). The authors also would like to thank the financial support from the State Key Laboratory of Ultra-precision Machining Technology and the Research Committee of The Hong Kong Polytechnic University (Project code: RK18).

**Data Availability Statement:** Not applicable.

**Conflicts of Interest:** The authors declare that they have no known competing financial interests or personal relationships that could have appeared to influence the work reported in this paper.

## References

1. Gautam, C.; Joyner, J.; Gautam, A.; Rao, J.; Vajtai, R. Zirconia based dental ceramics: Structure, mechanical properties, biocompatibility and applications. *Dalton Trans.* **2016**, *45*, 19194–19215. [[CrossRef](#)] [[PubMed](#)]
2. Mondal, B.; Chattopadhyay, A.B.; Virkar, A.; Paul, A. Development and performance of zirconia-toughened alumina ceramic tools. *Wear* **1992**, *156*, 365–383. [[CrossRef](#)]
3. Pantea, M.; Antoniac, I.; Trante, O.; Ciocoiu, R.; Fischer, C.A.; Traistaru, T. Correlations between connector geometry and strength of zirconia-based fixed partial dentures. *Mater. Chem. Phys.* **2019**, *222*, 96–109. [[CrossRef](#)]
4. Chen, H.; Ding, C.X. Nanostructured zirconia coating prepared by atmospheric plasma spraying. *Surf. Coat. Technol.* **2002**, *150*, 31–36. [[CrossRef](#)]
5. Pfefferkorn, F.E.; Shin, Y.C.; Tian, Y.; Incropera, F.P. Laser-assisted machining of magnesia-partially-stabilized zirconia. *J. Manuf. Sci. Eng.* **2004**, *126*, 42–51. [[CrossRef](#)]
6. Yin, L.; Jahanmir, S.; Ives, L.K. Abrasive machining of porcelain and zirconia with a dental handpiece. *Wear* **2003**, *255*, 975–989. [[CrossRef](#)]
7. Hocheng, H.; Kuo, K.L.; Lin, J.T. Machinability of Zirconia Ceramics in Ultrasonic Drilling. *Mater. Manuf. Process.* **1999**, *14*, 713–724. [[CrossRef](#)]
8. Juri, A.Z.; Zhang, Y.; Kotousov, A.; Yin, L. Zirconia responses to edge chipping damage induced in conventional and ultrasonic vibration-assisted diamond machining. *J. Mater. Res. Technol.* **2021**, *13*, 573–589. [[CrossRef](#)]
9. Camposilvan, E.; Leone, R.; Gremillard, L.; Sorrentino, R.; Zarone, F.; Ferrari, M.; Chevalier, J. Aging resistance, mechanical properties and translucency of different yttria-stabilized zirconia ceramics for monolithic dental crown applications. *Dent. Mater.* **2018**, *34*, 879–890. [[CrossRef](#)]
10. Tsugawa, K.; Ishihara, M.; Kim, J.; Hasegawa, M.; Koga, Y. Large-Area and Low-Temperature Nanodiamond Coating by Microwave Plasma Chemical Vapor Deposition. 2006. Available online: <https://www.researchgate.net/publication/236737100> (accessed on 30 May 2023).

11. Shen, B.; Sun, F. Effect of surface morphology on the frictional behaviour of hot filament chemical vapour deposition diamond films. *Proc. Inst. Mech. Eng. Part J J. Eng. Tribol.* **2009**, *223*, 1049–1058. [[CrossRef](#)]
12. Polini, R.; Mantini, F.P.; Braic, M.; Amar, M.; Ahmed, W.; Taylor, H. Effects of Ti- and Zr-based interlayer coatings on the hot filament chemical vapour deposition of diamond on high speed steel. *Thin Solid Films* **2006**, *494*, 116–122. [[CrossRef](#)]
13. Zhu, W.; Mccune, R.C.; Devries, J.E.; Tamor, M.A.; Ng, K.Y.S. Characterization of diamond films on binderless W-Mo composite carbide. *Diam. Relat. Mater.* **1994**, *3*, 1270–1276. [[CrossRef](#)]
14. Ehrhardt, H. New developments in the field of superhard coatings. *Surf. Coat. Technol.* **1995**, *74*, 29–35. [[CrossRef](#)]
15. Liu, H.; Dandy, D.S. Studies on nucleation process in diamond CVD: An overview of recent developments. *Diam. Relat. Mater.* **1995**, *4*, 1173–1188. [[CrossRef](#)]
16. Michler, J.; Stiegler, J.; von Kaenel, Y.; Moeckli, P.; Dorsch, W.; Stenkamp, D.; Blank, E. Microstructure evolution and non-diamond carbon incorporation in CVD diamond thin films grown at low substrate temperatures. *J. Cryst. Growth* **1997**, *172*, 404–415. [[CrossRef](#)]
17. Rozbicki, R.T.; Sarin, V.K. Nucleation and growth of combustion flame deposited diamond on silicon nitride. *Int. J. Refract. Met. Hard Mater.* **1998**, *16*, 377–388. [[CrossRef](#)]
18. Geng, D.; Zhang, D.; Xu, Y.; He, F.; Liu, F. Comparison of drill wear mechanism between rotary ultrasonic elliptical machining and conventional drilling of CFRP. *J. Reinf. Plast. Compos.* **2014**, *33*, 797–809. [[CrossRef](#)]
19. Xu, S.; Shimada, K.; Mizutani, M.; Kuriyagawa, T. Fabrication of hybrid micro/nano-textured surfaces using rotary ultrasonic machining with one-point diamond tool. *Int. J. Mach. Tools Manuf.* **2014**, *86*, 12–17. [[CrossRef](#)]
20. Singh, R.P.; Singhal, S. Investigation of machining characteristics in rotary ultrasonic machining of alumina ceramic. *Mater. Manuf. Process.* **2017**, *32*, 309–326. [[CrossRef](#)]
21. Wojciechowski, S.; Mrozek, K. Mechanical and technological aspects of micro ball end milling with various tool inclinations. *Int. J. Mech. Sci.* **2017**, *134*, 424–435. [[CrossRef](#)]
22. Kizaki, T.; Harada, K.; Mitsuishi, M. Efficient and precise cutting of zirconia ceramics using heated cutting tool. *CIRP Ann. Manuf. Technol.* **2014**, *63*, 105–108. [[CrossRef](#)]
23. Dong, X.; Zheng, L.; Wei, W.; Sun, X.; Liu, Z.; Sun, Y.; He, Z. Drilling force characteristics and casing drill wear analysis of GFRP low frequency axial vibration hole making. *Diam. Abras. Eng.* **2023**, *43*, 82–89. [[CrossRef](#)]
24. Peng, F.; Lei, D.; Wang, W. Diamond grinding quality analysis based on control grinding depth. *Diam. Abras. Eng.* **2023**, *43*, 118–125. [[CrossRef](#)]
25. Yang, C.; Zhang, N.; Su, H.; Ding, W. Research on abrasive wear of CBN Hinge honing Tool based on Single Abrasive Cutting. *Diam. Abras. Eng.* **2022**, *42*, 728–737. [[CrossRef](#)]
26. Neves, D.; Diniz, A.E.; Lima, M.S.F. Microstructural analyses and wear behavior of the cemented carbide tools after laser surface treatment and PVD coating. *Appl. Surf. Sci.* **2013**, *282*, 680–688. [[CrossRef](#)]
27. Osswald, S.; Yushin, G.; Mochalin, V.; Kucheyev, S.O.; Gogotsi, Y. Control of sp<sup>2</sup>/sp<sup>3</sup> carbon ratio and surface chemistry of nanodiamond powders by selective oxidation in air. *J. Am. Chem. Soc.* **2006**, *128*, 11635–11642. [[CrossRef](#)] [[PubMed](#)]
28. Das, D.; Singh, R.N. A review of nucleation, growth and low temperature synthesis of diamond thin films. *Int. Mater. Rev.* **2007**, *52*, 29–64. [[CrossRef](#)]
29. Bian, R.; He, N.; Ding, W.; Liu, S. A study on the tool wear of PCD micro end mills in ductile milling of ZrO<sub>2</sub> ceramics. *Int. J. Adv. Manuf. Technol.* **2017**, *92*, 2197–2206. [[CrossRef](#)]
30. Zhang, J.; Yuan, Y.; Zhang, J. Cutting performance of microcrystalline, nanocrystalline and dual-layer composite diamond coated tools in drilling carbon fiber reinforced plastics. *Appl. Sci.* **2018**, *8*, 1642. [[CrossRef](#)]
31. Yuan, Z.; Guo, Y.; Li, C.; Liu, L.; Yang, B.; Song, H.; Zhai, Z.; Lu, Z.; Li, H.; Jiang, X.; et al. New multilayered diamond/ $\beta$ -SiC composite architectures for high-performance hard coating. *Mater. Des.* **2020**, *186*, 108207. [[CrossRef](#)]
32. Carroll, L.J.; Cabet, C.; Carroll, M.C.; Wright, R.N. The development of microstructural damage during high temperature creep-fatigue of a nickel alloy. *Int. J. Fatigue* **2013**, *47*, 115–125. [[CrossRef](#)]

**Disclaimer/Publisher's Note:** The statements, opinions and data contained in all publications are solely those of the individual author(s) and contributor(s) and not of MDPI and/or the editor(s). MDPI and/or the editor(s) disclaim responsibility for any injury to people or property resulting from any ideas, methods, instructions or products referred to in the content.